Optimal Rotor Poles and Structure for Design of Consequent Pole Permanent Magnet Flux Switching Machine

Wasiq Ullah[*], *Faisal Khan and Muhammad Umair*
(Department of Electrical and Computer Engineering, COMSATS University Islamabad (Abbottabad Campus), Abbottabad 22040, Pakistan)

Abstract: Permanent magnet flux switching machines (PMFSM) have attracted significant research interest and are considered as competent candidates when higher torque density is primary requirement. However, conventional PMFSMs uses excessive rare earth PM volumes which ultimately increases machine the machine weight and PM cost. Moreover, the PMs extended at the stator yoke results in stator leakage flux which degrades the performance. To suppress the leakage flux and diminish the PM volume, the consequent pole PMFSM (CPPMFSM) with flux bridges and barriers encompassing partitioned circumferential and radial magnetized PMs is proposed, thereby ensuring an alternate magnetic path for the working harmonics which improves the modulation effect and flux distribution. Moreover, the influence of the rotor pole number on seven different rotor structures namely, curved rotor, trapezoidal rotor, wide rotor tooth tip, wide rotor base width, rectangular segmented and eccentric rotors are investigated based on the electromagnetic performance and stress distribution. Finite element analysis (FEA) reveals that the 12S-13P CPPMFSM with a wider rotor base offers comparatively better electromagnetic performance. Compare to the conventional PMFSM, the proposed CPPMFSM reduces the PM volume which minimizes the overall machine cost and weight, suppresses the torque ripples by 16.49%, diminishes total harmonic distortion (THD) by 35.24% and decreases cogging torque by 32.88%. Furthermore, the torque and power density are enhanced by 7.028% and 7.025% respectively.

Keywords: AC Machine, consequent pole, flux bridge, flux switching machine, permanent magnet, rotor pole number, rotor structure, stress analysis

1 Introduction

Permanent magnet flux switching machine (PMFSM) houses both concentrated armature windings and permanent magnets (PMs) in the stator, yielding a simple robust rotor made of iron only. PMFSM combine features of switched reluctance machine and permanent magnet synchronous machine. Owing to their double salient structure and sinusoidal back electromotive force (EMF), PMFSMs are considered as feasible candidates for direct drive high speed brushless applications, including domestic and industrial applications [1], electric vehicle traction [2], wind applications [3-4], hybrid electric vehicles [5], and automotive industry [6]. PMFSMs are preferable for the above-mentioned applications when primitive requisites are high torque and power density. However, PMFSMs uses high rare-earth PM volume as the main excitation source which increases the overall machine weight and cost.

In PMFSM, despite of the high volume of the PM usage, the alternate polarities and circumferentially magnetized PMs sandwich between armature coils in the stator are extended to outer radius of stator which cause serious issue of the flux leakages in the surrounding instead of linking through stator yoke as illustrated in Fig. 1 [2]. Various studies have reported reduced PM use machines and suppression of leakage flux. Ref. [7] investigated reduced PM machines and the effect of mechanical flux adjustor for stator leakage flux was investigated in Ref. [8]. However, mechanical flux adjustor requires additional accessories which increase

Manuscript received July 12, 2020; revised October, 26, 2020; accepted February 25, 2021. Date of publication March 31, 2021; date of current version March 4, 2021.
* Corresponding Author, E-mail: wasiqullah014@gmail.com
Digital Object Identifier: 10.23919/CJEE.2021.000011

machine weight and cost. Ref. [9] suppressed flux leakages through consequent pole (as shown in Fig. 2a) but failed to reduce the PMs volume. To overcome the issues of both high PM usage and stator leakage flux, this paper propose consequent pole PMFSM (CPPMFSM) incorporated an E-core stator slot with flux bridge and flux barriers as depicted in Fig. 2b.

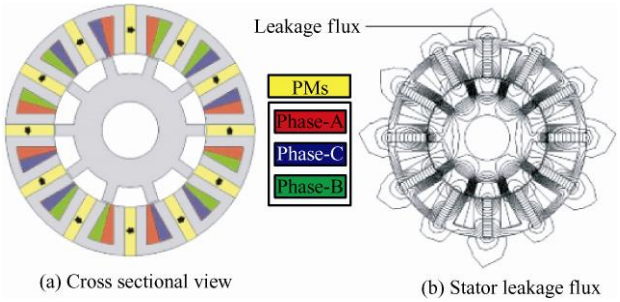

Fig. 1 PMFSM

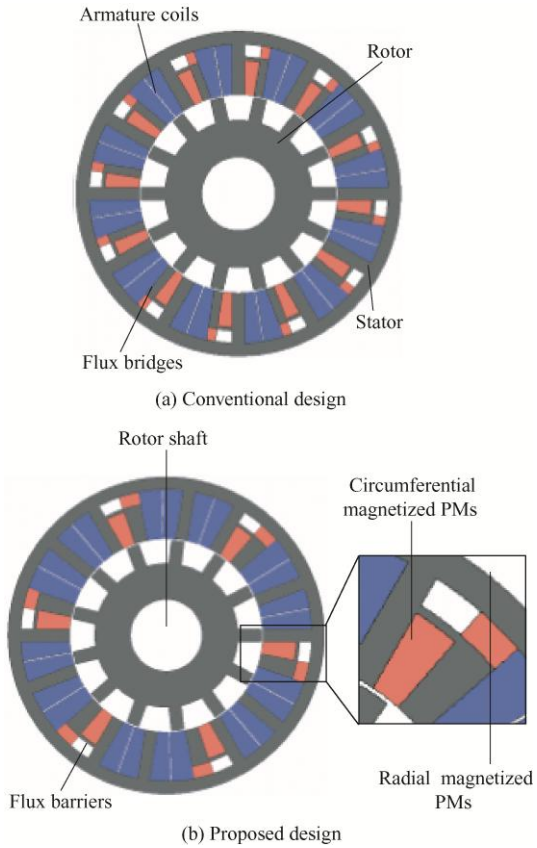

Fig. 2 Cross sectional view of CPPMFSM

Main contributions of this paper are as follow: (a) the PM volume is reduced by 46.53%; (b) the PM cost is minimize by 30.69%; (c) the overall machine weight is reduced by 6.01%; and (d) a feasible rotor pole study is carried out on seven different rotor structures. A comprehensive electromagnetic performance analysis is conducted on rotor poles and structure for CPPMFSM design.

The remain of this paper is organized as follow, Section 2 describes the operating principle of CPPMFSM. Optimal rotor pole and rotor structures are investigated in Section 3. Section 4 analyze electromagnetic performance of rotor topologies and Section 5 investigates stress analysis on rotor structure, Section 6 present comparison of conventional and proposed design. Finally, several conclusions are drawn in Section 7.

2 Operating principle of CPPMFSM

Conventional and proposed model are design using design parameters listed in Tab. 1 and shown in Fig. 3. CPPMFSM housed partitioned radial magnetized (RM) and circumferentially magnetized (CM) PMs above and below laminated h-shaped salient pole in E-core stator slot. PMs are enclosed with flux barriers and flux bridges below stator yoke which provides alternate path to the main flux passing through stator yoke hence suppressing the flux leakages and improving flux modulation.

Tab. 1 Design parameters of CPPMFSM

Design parameter	Conventional	Proposed
PMs volume V_{PM}/mm^3	11 856.54	8 091.25
PM outer radius R_{PM}/mm	—	37
Stator outer radius R_{os}/mm	45	
Inner radius of stator R_{si}/mm	27.5	
Inner radius of rotor R_{ri}/mm	20.4	
Outer radius of stator R_{or}/mm	27	
Pole width R_{rtw}/mm	4	
Width of stator slot R_{stw}/mm	4	
Radius of shaft R_{sr}/mm	10.2	
Conductor per phase	180	

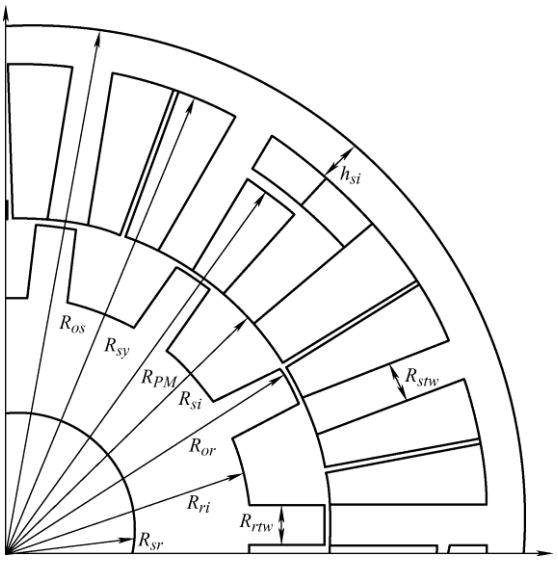

Fig. 3 Design parameters of CPPMFSM

Operating principle of CPPMFSM for one periodic cycle based on finite element analysis (FEA) flux distribution with the aid of an open-circuit flux distribution of one coil (A1) is depicted in Fig. 4. It can be clearly observed from Fig. 4a and Fig. 4c that the maximum flux linkages occur when the rotor poles are aligned to the right or left tooth of stator pole A1 at *d*-axis position, respectively. Moreover, zero-flux linkage is obtained when rotor pole is symmetric to stator slot *q*-axis. Note that rotor changes its position from Fig. 4a-Fig. 4c. the flux linkage becomes bi-polar. A typical flux linkage over one periodic cycle is illustrated in Fig. 5.

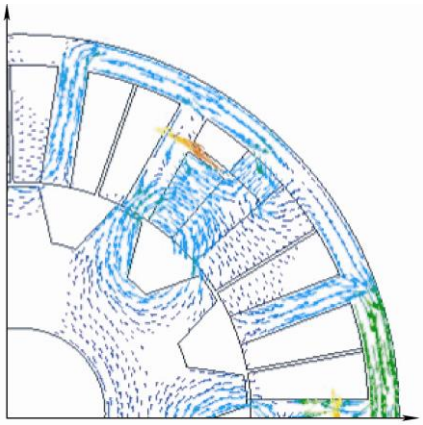

(a) Rotor at negative *d*-axis position

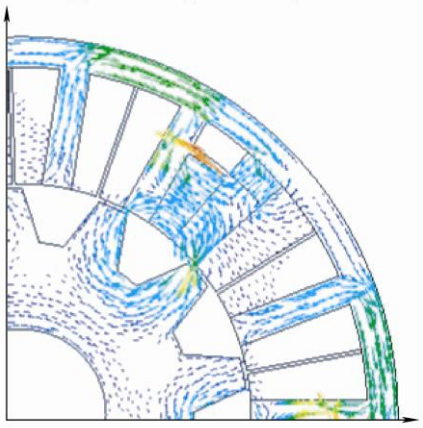

(b) Rotor at negative *q*-axis position

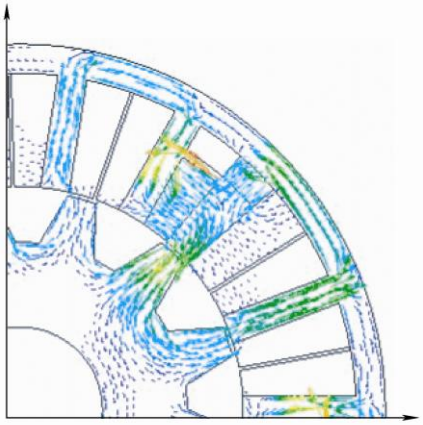

(c) Rotor at positive *d*-axis position

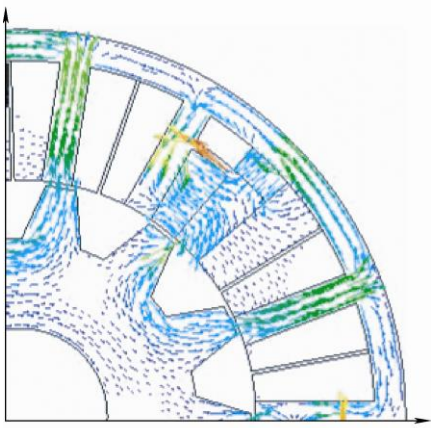

(d) Rotor at positive *q*-axis position

Fig. 4 Open-circuit flux distribution of CPPMFSM

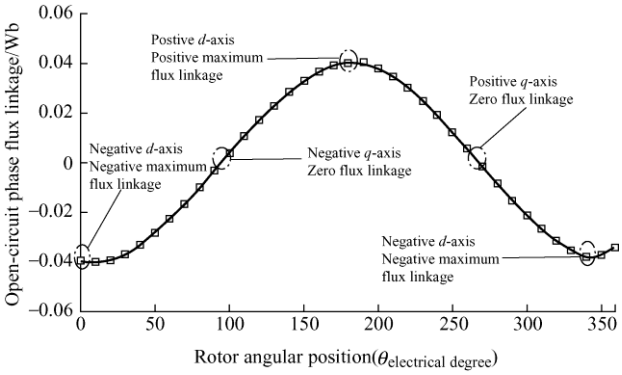

Fig. 5 Typical open-circuit phase flux linkage of CPPMFSM in one periodic cycle

Furthermore, the magnetic field harmonics of the conventional and proposed design are shown in Fig. 6. It can be clearly observed that the addition of RM-PMs and CM-PMs in proposed design improves the working harmonic contents owing to superposition occurring in flux modulation that enhance electromagnetic performance.

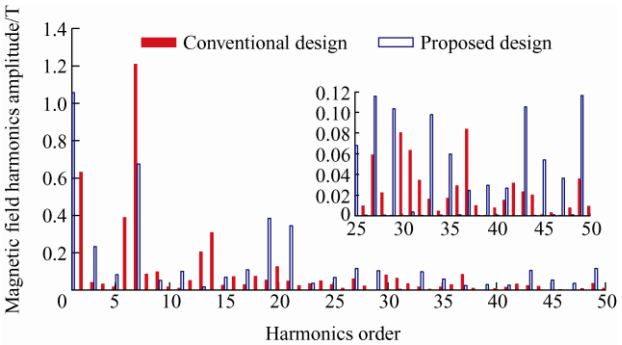

Fig. 6 Magnetic field harmonics

3 Optimal rotor pole and rotor structure

3.1 Combination of stator slot and rotor poles

During the initial design phase, it's mandatory to determine the optimal stator and rotor pole combination

to achieve high torque density and improve electromagnetic performance. The electromagnetic properties such as torque density and power density vary significantly for any model with different stator slot (Z_s) and rotor pole numbers (Z_r). A wide range of feasible rotor pole combinations exist for any electric machine. The feasible combinations stator slots and rotor poles for a three-phase CPPMFSM can be determined using Eq. (1) and Eq. (2).

$$Z_s = km \tag{1}$$

$$Z_r = 2Z_s \pm k \tag{2}$$

whereas k is an integer and m represents the number of phases.

For different values of k, various rotor pole and stator slot such as Z_s/Z_r=12/8, 12/9, 12/10, 12/11, 12/13, 12/14, 12/15, 12/16, and 12/17 are developed, simulated and analyzed under 2-D FEA. Based on no-test and on-load conditions, designs with that Z_s/Z_r=12/11, 12/13, and 12/17, are capable of producing sinusoidal open-circuit phase flux linkage and uni-directional instantaneous torque [10-11]. Therefore, aforesaid three rotor poles are proceeded to rotor structure.

3.2 Rotor structure

The selected optimal number of stator slot rotor pole Z_s/Z_r=12/11, 12/13, and 12/17 is analyzed for the feasible rotor structure to achieve better electromagnetic performance such higher torque density, power density, higher average torque, lower torque ripples, low cogging torque. For this purpose, seven different types of the rotor structure, i.e., curved rotor (CR), trapezoidal rotor (TR), wide rotor tip width (WRTW), wide rotor base width (WRBW), rectangular rotor (RR), segmented rotor (SR), and eccentric rotors (ER) are developed as shown in Fig. 7a-Fig. 7g.

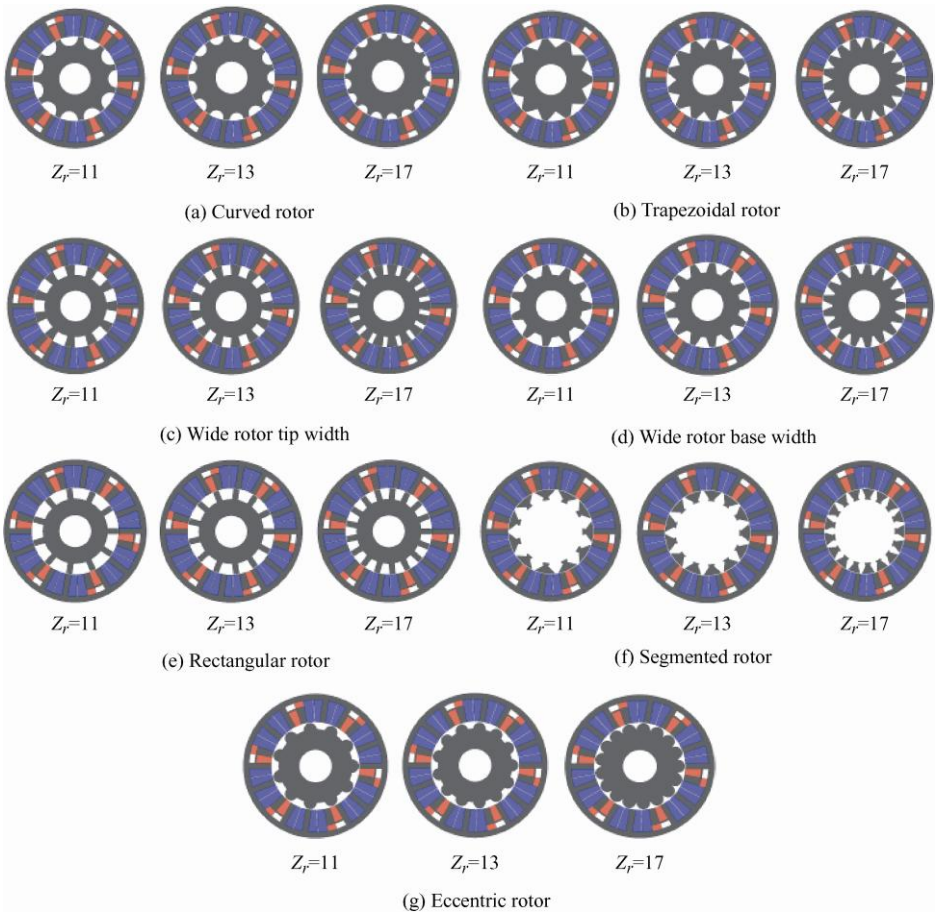

Fig. 7 Rotor structure

A comprehensive overview of electromagnetic performance of the aforesaid rotor structure with key performance indicators, i.e., peak to peak open-circuit phase flux linkage ($\Phi_{p\text{-}p}$), cogging torque (T_{cog}), average torque (T_{avg}), torque ripples (T_{rip}), open-circuit phase flux linkage total harmonics distortion (Φ_{THD}), average power (P_{avg}), torque density (T_{den}), and power density (P_{den}) are listed in Tab. 2. Analysis reveals that Z_r=13 offer comparatively better electromagnetic performance, therefore, proceeded to electromagnetic comparison.

Tab. 2 Detailed electromagnetic performance of various rotor topologies for design of CPPMFSM

S.No	Rotor structure	Z_s	Z_r	$\Phi_{p\text{-}p}$ /Wb	T_{cog} /(N·m)	T_{avg} /(N·m)	T_{rip} /(N·m)	Φ_{THD} (%)	P_{avg} /W	T_{den} /(kN·m/kg)	P_{den} /(kW/kg)
1	Curved	12	11	0.035	1.603	1.139	2.286	7.066 7	259.95	125.43	16.614 0
			13	0.081	1.686	2.536	3.077	1.107 3	388.59	279.25	36.986 0
			17	0.053	2.099	1.736	6.945	66.148 0	435.39	191.21	25.325 0
2	Trapezoidal	12	11	0.032	1.474	1.093	2.013	5.857 2	254.08	120.36	15.942 0
			13	0.078	1.644	2.449	3.047	1.094 7	380.15	269.66	35.717 0
			17	0.054	1.978	1.021	5.364	65.730 0	220.74	112.44	14.893 0
3	Wide rotor tip width	12	11	0.033	0.472	1.278	1.419	9.038 5	280.25	140.71	18.637 0
			13	0.071	2.265	2.161	3.819	4.157 0	350.36	237.93	31.513 0
			17	0.034	2.499	0.563	4.345	65.681 0	171.40	62.006	8.212 8
4	Wide rotor base width	12	11	0.034	1.584	1.127	2.054	6.881 8	257.93	124.09	16.436 0
			13	0.080	1.715	2.556	3.113	1.358 4	389.84	281.55	37.291 0
			17	0.054	2.001	1.032	5.411	65.653 0	221.77	113.66	15.054 0
5	Rectangular	12	11	0.034	1.586	1.080	2.155	6.311 2	251.65	118.97	15.758 0
			13	0.079	1.693	2.403	3.002	1.390 7	353.33	264.71	35.060 0
			17	0.054	1.999	1.032	5.312	65.977 0	218.81	113.61	15.048 0
6	Segmented	12	11	0.029	1.045	0.682	2.381	1.653 2	194.45	75.104	9.947 5
			13	0.011	0.978	0.607	1.848	8.795 9	170.21	66.797	8.847 3
			17	0.031	0.811	0.985	1.586	47.343 0	76.324	108.480	0.043 5
7	Eccentric	12	11	0.013	0.437	0.564	1.377	4.914 9	188.34	62.066	8.220 6
			13	0.023	0.964	0.894	2.371	2.364 6	211.60	98.443	13.039 0
			17	0.020	0.566	0.577	1.853	72.544 0	139.62	63.494	8.409 8

4 Electromagnetic performance omparison of rotor structures

Detailed electromagnetic performance of rotor structure is investigated with key performance indicator such as $\Phi_{p\text{-}p}$, T_{cog}, T_{avg}, T_{rip}, Φ_{THD}, P_{avg}, T_{den}, and P_{den} which show that CPPMFSM with 13 rotor poles exhibits better electromagnetic performance.

4.1 Open circuit phase flux linkage

Open-circuit phase flux linkage for seven various rotor structures are shown in Fig. 8. Enlarge portion shows that peak values of flux linkages for all rotor types are nearly equal without ER and SR which offer least open circuit flux linkages. Detail $\Phi_{p\text{-}p}$ are listed in Tab. 2. Detail analysis unveil that CR followed by WRBW offer higher peak to peak open-circuit phase flux linkages whereas ER followed by SR offer least phase flux linkage.

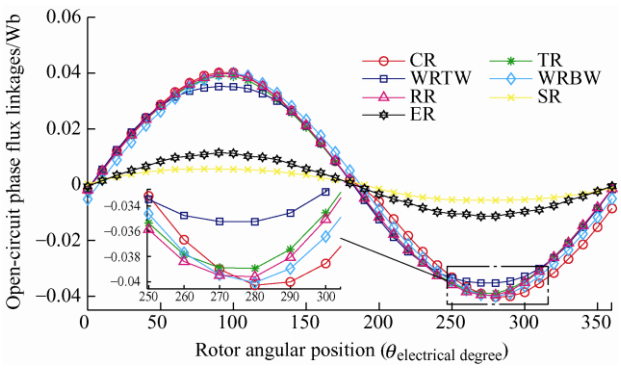

Fig. 8 Open-circuit phase flux linkage of rotor topologies

4.2 Cogging torque

Torque under no-load condition, i.e., I_a=0 A is referred to be cogging torque. It is undesirable since it results in acoustic noise and vibration. Cogging torque for different rotor topologies in CPPMFSM is shown in Fig. 9. Analysis reveals that T_{cog}, for ER followed by WRBW is lower however, the electromagnetic performance listed in Tab. 2 shows that ER offer lower torque and WRBW offer highest torque.

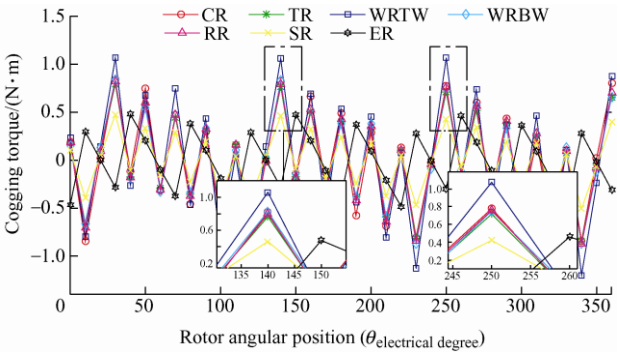

Fig. 9 Cogging torque for different rotor topologies

4.3 Instantaneous torque

Torque generated at each instant when armature current is applied, this torque is known as Instantaneous torque. Fig. 10 shows ER shows least torque and WRTW exhibits higher ripples content. Detail analysis listed in Tab. 2 shows that the highest torque is generated by WRWB followed by CR.

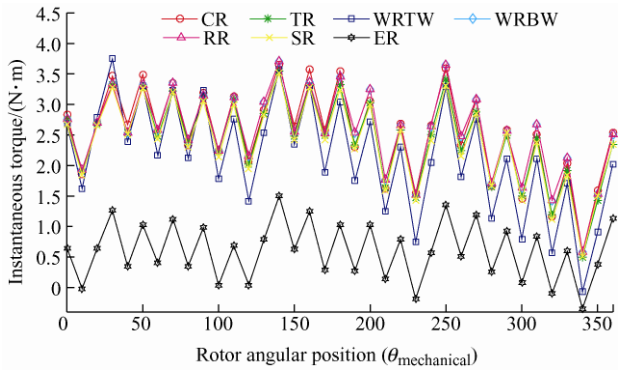

Fig. 10 Instantaneous torque response for various rotor structure

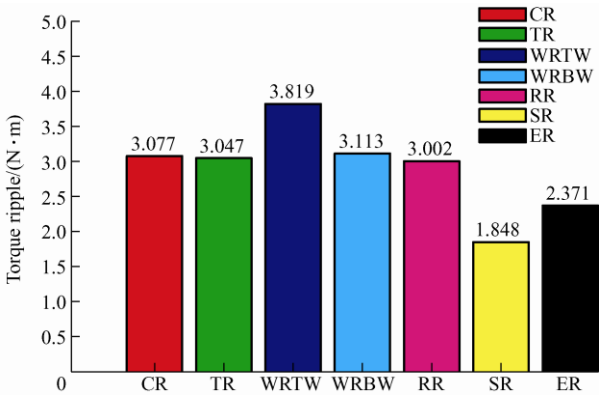

Fig. 11 Torque ripples of CPPMFSM with 13 rotor pole for various rotor topologies

4.4 Total harmonic distortion of flux linkage

THD is computed for open-circuit phase flux linkage of various rotor topologies of CPPMFSM. THD for different rotors is calculated by fast Fourier transform (FFT) followed by Eq. (3)

$$\Phi_{THD} = \frac{\sqrt{\sum_{i=2}^{N} U_i^2}}{U_1} \tag{3}$$

where U_1 and U_i refer to fundamental and harmonics order of the phase U respectively.

Analysis reveals that least Φ_{THD} of 1.10% is obtained in CPPMFSM with TR render whereas CR, WRBW and RR offer moderate harmonic distortion in the open-circuit phase flux linkages.

4.5 Torque ripple

Torque ripple (T_{rip}), is the difference of the maximum torque peak ($T_{\max}$) and minimum torque peak ($T_{\min}$) at the instantaneous torque response given as Eq. (4)

$$T_{rip} = T_{\max} - T_{\min} \tag{4}$$

The torque ripples for various rotors are shown in Fig. 11 and listed in Tab. 2 shows that CPPMFSM with ER structure with 11 rotor poles offer lowest torque ripples of 1.38 N·m whereas other topologies such as SR, CR, TR, RR and WRBW offered moderate ripples content as shown in Fig. 11 for 13 rotor poles. Since torque ripples are higher than average torque it is suppressed utilizing harmonic injection in Ref. [12].

4.6 Torque density and power density

Torque and power densities are considered as the major key performance indicator in the design of PM machines. It shows PM contribution in the torque and power generated which is give in Eq. (5) and Eq. (6)

$$T_{den}=T_{avg}/V_{PM} \tag{5}$$

$$P_{den}=P_{avg}/M_{PM} \tag{6}$$

whereas P_{avg} is average power and M_{PM} is total PM mass.

Analysis reveals that CPPMFSM with WRBW offer the highest torque density and power density of 281.55 kN·m/m^3 and 37.29 kW/kg respectively whereas lowest offered by CPPMFSM with SR as shown in Fig. 12 and Fig. 13 respectively for 13 rotor poles.

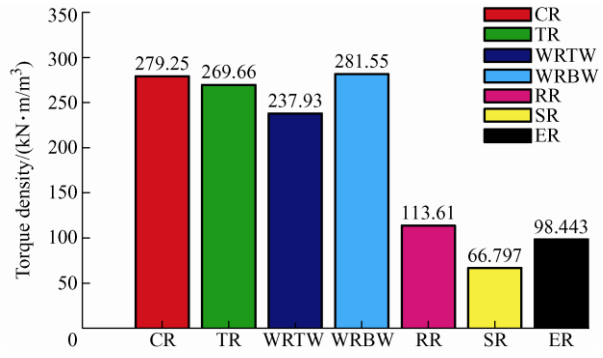

Fig. 12 Torque density of CPPMFSM with rotor topologies

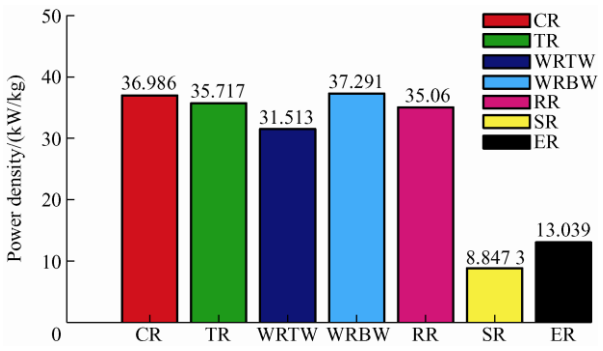

Fig. 13 Power density of CPPMFSM with rotor topologies

5 Rotor stress analysis

This analysis technique is employed to investigate principal stress occurred in various rotor structures as developed for various rotor structure for design of CPPMFSM. Stress analysis on rotor is conducted in such a way that actual condition and constraints are applied in accordance with the material characteristics. Since rotor is subjected to centrifugal rolling force therefore, mechanical stress condition of rotor structure is accomplished by centrifugal force due to longitudinal rotor rotation [13]. This centrifugal force is greatly influenced by angular rotating velocity of rotor therefore analysis is carried out in the wide range of angular velocity to investigate variation of principal stress in various rotor pole shaping methods. In order to examine principal stress on rotor, constraints are set on rotor that coincides to the force acting on rotor pole, rotor tip and rotor back iron (rotor shaft) as shown in Fig. 14 with the overall flow chart of analysis in Fig. 15.

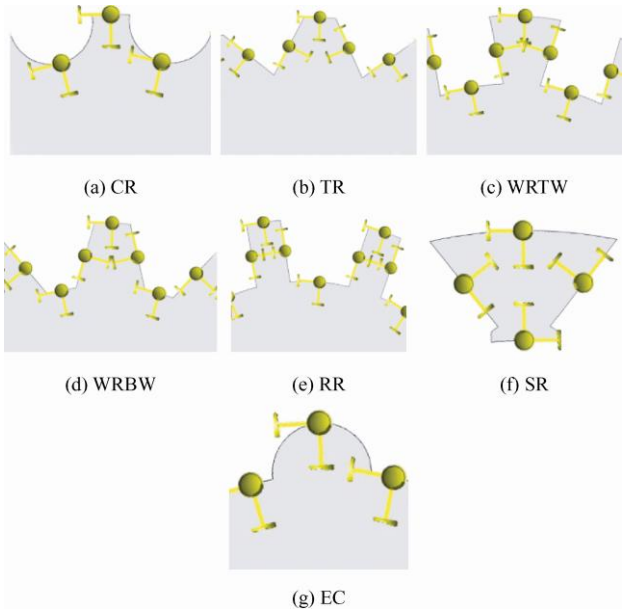

Fig. 14 Constraints on rotor for stress analysis

Since principal stress on rotor varies with rotating angular speed therefore, analysis is carried out from 0 to 30 000 r/min with difference of 3 000 r/min.

Fig. 16 shows Nephogram of principal stress on various rotor pole shapes at 30 000 r/min whereas it's variation with speed is illustrated in Fig. 17. This mechanical study of principal stress is carried out on rotor for conventional electromagnetic steel 35H210 having maximum allowable principal stress of 300 MPa.

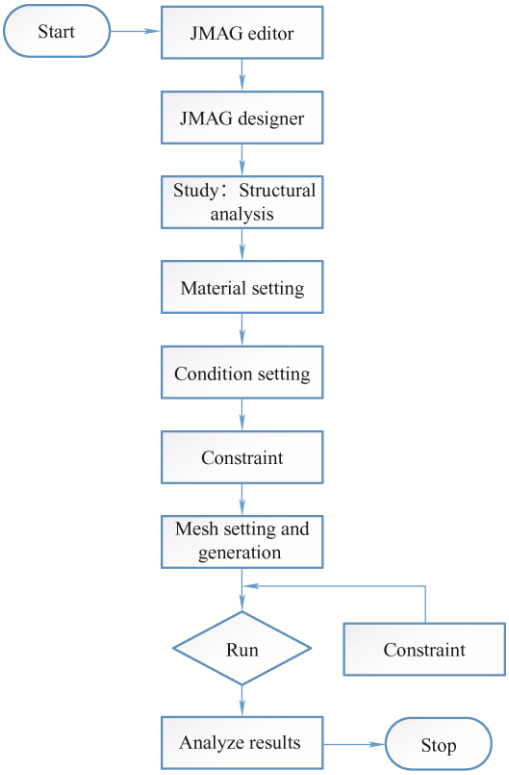

Fig. 15 Flow chart for rotor stress analysis

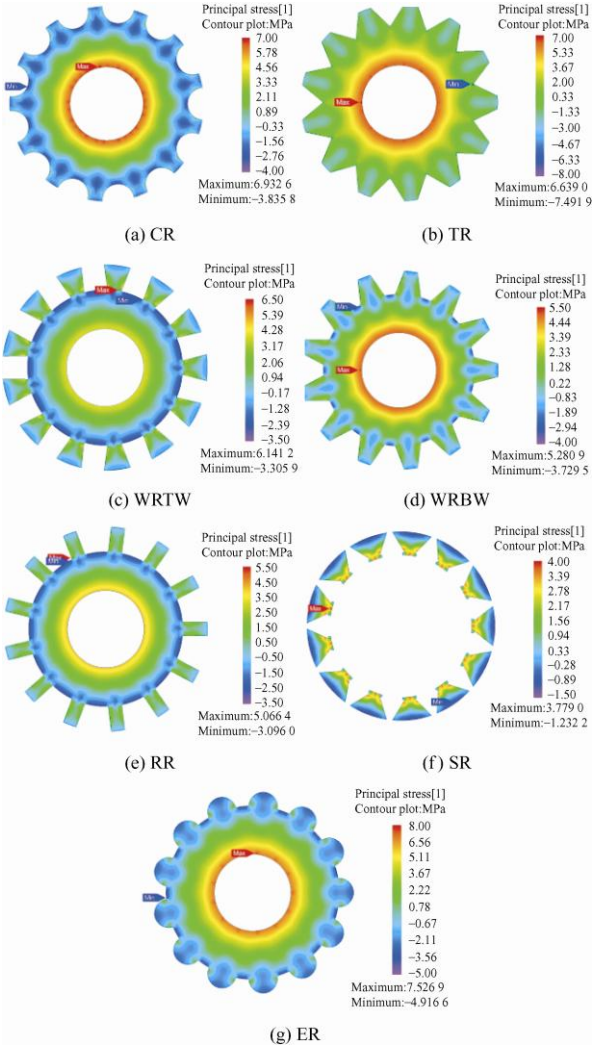

Fig. 16 Nephogram of principal stress at 30 000 r/min

It is worth mentioning that higher the principal stress for rotor, higher will be the withstand capability [14]. Based on variation of principal stress with rotating speed as shown in Fig. 17 and listed in Tab. 3, analysis reveals that with the change in rotating speed, principle stress is exponentially increasing. It can be clearly seen that ER offer highest withstand capability whereas CR, TR, WRTW and WRBW shows intermediate withstand capability. Thus, it is concluded that despite of suppressing torque ripples and diminishing cogging torque, rotor structures improve principal stress withstand capabilities, ensure its safe operation under higher speed and make it feasible for high speed applications. Note that smaller the principle stress better is machine safety.

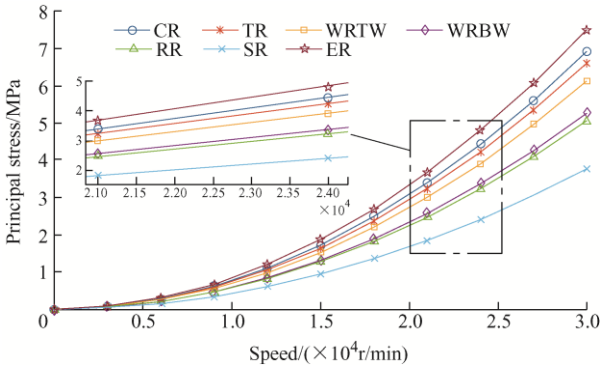

Fig. 17 Variation of principal stress with rotating angular velocity

Tab. 3 Variation of principal stress with speed

Speed /(r/min)	Principal stress on rotor/MPa						
	CR	TR	WRTW	WRTB	RR	SR	ER
0	0	0	0	0	0	0	0
3 000	0.069	0.06	0.061 4	0.052	0.050	0.037	0.075
6 000	0.277	0.26	0.245 6	0.211	0.202	0.151	0.301
9 000	0.623	0.59	0.557 0	0.475	0.457	0.340	0.677
12 000	1.109	1.06	0.982 6	0.844	0.810	0.604	1.204
15 000	1.733	1.65	1.535 3	1.320	1.277	0.944	1.881
18 000	2.495	2.39	2.210 0	1.901	1.823	1.360	2.709
21 000	3.397	3.25	3.009 0	2.587	2.482	1.851	3.882
24 000	4.436	4.24	3.903 0	3.379	3.242	2.418	4.817
27 000	5.615	5.37	4.974 0	4.277	4.103	3.061	6.096
30 000	6.932	6.63	6.140 0	5.280	5.066	3.779	7.526

6 Performance comparison of conventional and proposed design

In this section, CPPMFSM with 13 poles WRBW rotor is selected as optimal design which is to be compared with the existing conventional design with major key performance indicators such as cogging torque, torque ripples, Φ_{THD}, torque and power density.

Detailed quantitative electromagnetic performance of conventional and proposed model is listed in Tab. 4 whereas weight and cost are listed in Tab. 5. It can be clearly seen that overall weight is reduced by 6.01% whereas PM cost is reduced by 30.69%.

From Fig. 18 and Fig. 19, it can be clearly seen that conventional design back-EMF have higher harmonics content in comparison with the proposed design. Moreover, comparison of cogging torque profile in Fig. 20 reveals that propose CPPMFSM truncate cogging torque to 1.715 N·m from 2.555 2 N·m. Moreover, it can be clearly seen that cogging torque of proposed design is symmetrical and cancel out its effect in one periodic cycle. Thus, proposed design suffers from least vibration and acoustic noise due to lower interaction of PMs and armature slot.

Tab. 4 Quantitative electromagnetic performance comparison of conventional and proposed CPPMFSM

Key performance indicators	Conventional design	Proposed design
$\Phi_{p\text{-}p}$/Wb	0.100 09	0.080 0
T_{cog}/(N·m)	2.555 20	1.715 0
T_{avg}/(N·m)	3.119 00	2.556 0
T_{rip}/(N·m)	3.727 90	3.113 0
Φ_{THD}(%)	2.097 50	1.358 4
T_{den}/(kN·m/m^3)	263.060 00	281.550 0
P_{den}/(kW/kg)	34.843 00	37.291 0

Tab. 5 Comparison of conventional and proposed CPPMFSM machine weight and PM cost

Machine parts	Conventional design	Proposed design
PM volume/mm^3	11 856.00	8 091.25
PM weight/g	93	63
Stator weight/g	371	363
Rotor weight/g	251	246
Total weight/g	715	672
PM cost/$	13.13	9.10

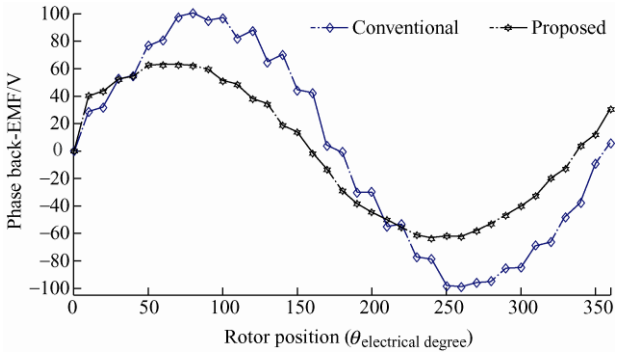

Fig. 18 Phase back-EMF wave form

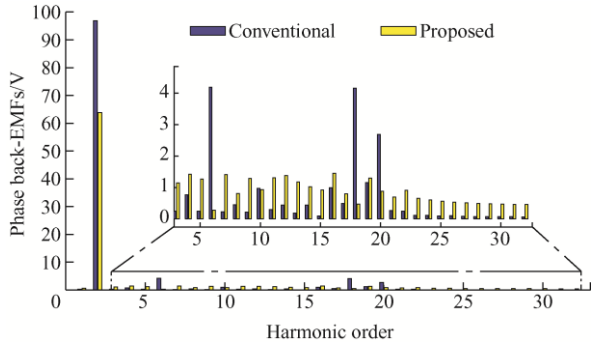

Fig. 19 Phase back-EMF spectra

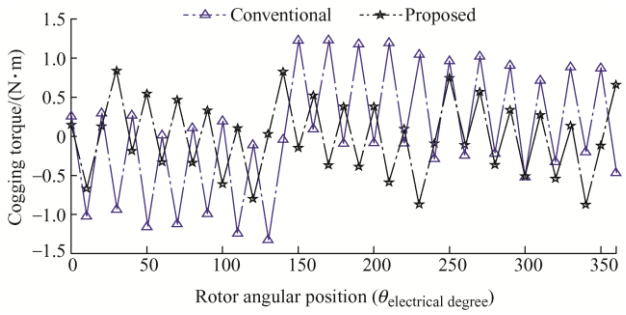

Fig. 20 Investigation of cogging torque in conventional and proposed design

Moreover, desirable instantaneous torque of conventional and proposed model is compared in Fig. 21. Analysis shows that initial design of proposed model offer slightly lower torque with lower peak values thus reducing torque ripples at the cost of average torque. However, this torque will be improved in the future using optimization techniques.

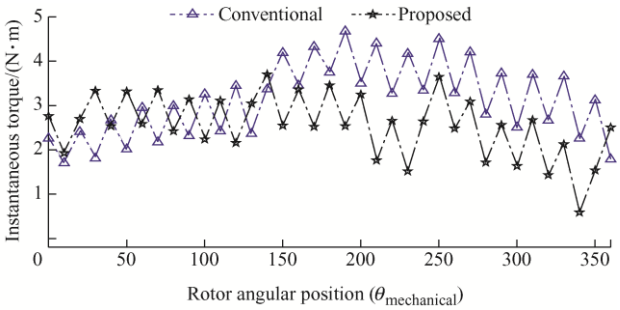

Fig. 21 Comparison of instantaneous torque for conventional and proposed design

Moreover, details electromagnetic performances of conventional and proposed design are listed Tab. 4. Analysis declared that despite of cogging torque and torque ripples reduction, proposed model successfully reduces Φ_{THD} and enhance torque and power density and reduce PM usage which reduces machine weight and PM cost.

7 Conclusions

In this paper, a low-cost E-core stator slot CPPMFSM with partitioned radial and circumferential magnetized PM's enclosed in flux bridges and flux barriers has been proposed. The proposed model enhances the flux modulation by providing alternate magnetic path to the working harmonics. An optimal stator slot and rotor pole study was carried out, followed by electromagnetic performance and stress analysis on seven different rotor topologies. Detail FEA analysis reveals that CPPMFSM with WRBW offers comparatively better electromagnetic performance. Compared to the conventional model, the proposed CPPMFSM enhanced torque density by 7.028%, improve power density by 7.025%, reduced PM utilization by 46.53%, suppressed torque ripples by 16.49%, diminished Φ_{THD} by 35.24%, and truncated cogging torque by 32.88% leading to reduced acoustic noise and vibration.

References

[1] T L Tiang, D Ishak, C P Lim, et al. A comprehensive analytical subdomain model and its field solutions for surface-mounted permanent magnet machines. *IEEE Trans. Magn.*, 2015, 51(4): 1-14.

[2] N Ullah, F Khan, W Ullah, et al. Analytical modelling of open-circuit flux linkage, cogging torque and electromagnetic torque for design of switched flux

permanent magnet machine. *Journal of Magnetics*, 2018, 23(2): 253-266.

[3] N Ullah, F Khan, W Ullah, et al. Magnetic equivalent circuit models using global reluctance networks methodology for design of permanent magnet flux switching machine. *2018 15th International Bhurban Conference on Applied Sciences and Technology (IBCAST), Islamabad*, 2018: 397-404.

[4] J T Chen, Z Q Zhu, S Iwasaki, et al. A novel E-core switched-flux PM brushless AC machine. *IEEE Trans. Ind. Appl.*, 2011, 47(3): 1273-1282.

[5] Z Q Zhu, L J Wu, Z P Xia. An accurate subdomain model for magnetic field computation in slotted surface-mounted permanent-magnet machines. *IEEE Trans. Magn.*, 2010, 46(4): 1100-1115.

[6] L I Jusoh, E Sulaiman, R Kumar, et al. Design and performance of 8S1ot-12Pole permanent magnet flux switching machines for electric bicycle application. *International Journal of Power Electronics and Drive Systems (IJPEDS)*, 2017, 8(1): 248-254.

[7] Z Q Zhu, J T Chen. Advanced flux-switching permanent magnet brushless machines. *IEEE Transactions on Magnetics*, 2010, 46(6): 1447-1453.

[8] Z Q Zhu, M M J Al-ani, X Liu, et al. Comparison of alternate mechanically adjusted variable flux switched flux permanent magnet machines. *2012 IEEE Energy Conversion Congress and Exposition (ECCE)*, *Raleigh, NC*, 2012: 3655-3662.

[9] Y Gao, D Li, R Qu, et al. Analysis of a novel consequent-pole flux switching permanent magnet machine with flux bridges in stator core. *IEEE Transactions on Energy Conversion*, 2018, 33(4): 2153-2162.

[10] W Ullah, F Khan, N Ullah, et al. Comparative study between C-core/E-core SFPMM with consequent pole SFPMM. *2019 International Symposium on Recent Advances in Electrical Engineering (RAEE)*, Islamabad, Pakistan, 2019: 1-6.

[11] U Wasiq, K Faisal, S Erwan, et al. Analytical validation of novel consequent pole E-core stator permanent magnet flux switching machine. *IET Electric Power Applications*, 2020, 14(5): 789-796.

[12] W Ullah, F Khan, E Sulaiman, et al. Torque characteristics of high torque density partitioned PM consequent pole flux switching machines with flux barriers. *CES Transactions on Electrical Machines and Systems*, 2020, 4(2): 130-141.

[13] J A Rani, E Sulaiman, M F Omar, et al. Computational method of rotor stress analysis for various flux switching machine using J-MAG. *2015 IEEE Student Conference on Research and Development (SCOReD)*, Kuala Lumpur, 2015: 721-726.

[14] L U Rahman, F Khan, M A Khan, et al. Modular rotor single phase field excited flux switching machine with non-overlapped windings. *Energies*, 2019, 12(8): 1576-1603.

Wasiq Ullah is from Afghanistan and was born in District Peshawar, Khyber Pakhtunkhwa, Pakistan in 1995. He received his B.S. and M.S. degrees in electrical (power) engineering from COMSATS University Islamabad (Abbottabad Campus), Abbottabad, Pakistan in 2018 and 2020 respectively. He is currently pursuing his PhD degree in electrical (power) engineering from COMSATS University Islamabad (Abbottabad Campus), Abbottabad, Pakistan.

From 2018, he has been research associate with electric machine design research group. His research interests include analytical modelling, design analysis and optimization of permanent magnet flux switching machines, linear flux switching machines, hybrid excited flux switching machines and novel consequent pole flux switching machines for high speed brushless AC applications.

Faisal Khan was born in District Charsadda, Khyber Pakhtunkhwa, Pakistan in 1986. He received his B.S. degree in electronics engineering from COMSATS University Islamabad (Abbottabad Campus), Pakistan in 2009 and his M.S. degree in electrical engineering from COMSATS University Islamabad (Abbottabad Campus), Pakistan in 2012. He received his Ph.D. degree in electrical engineering from Universiti Tun Hussein Onn Malaysia, Malaysia in 2017.

From 2010 to 2012, he was a lecturer at the University of Engineering & Technology, Abbottabad, Pakistan. Since 2017, he has been as assistant professor with the Electrical Engineering Department, COMSATS University Islamabad (Abbottabad Campus), Pakistan. He is the author of more than 70 publications, one patent, and has received multiple research awards. His research interests include design and analysis of flux-switching machines, synchronous machines, and DC machines.

Muhammad Umair was born in District Peshawar, Khyber Pakhtunkhwa, Pakistan in 1995. He received his B.S. degrees in electrical (power) engineering from COMSATS University Islamabad (Abbottabad Campus), Abbottabad, Pakistan in 2018. He is currently pursuing his M.S degree in electrical (power) engineering at COMSATS University Islamabad (Abbottabad Campus). His research interests include the design, analysis, optimization and experimental validation of flux-switching machines.